PAPER

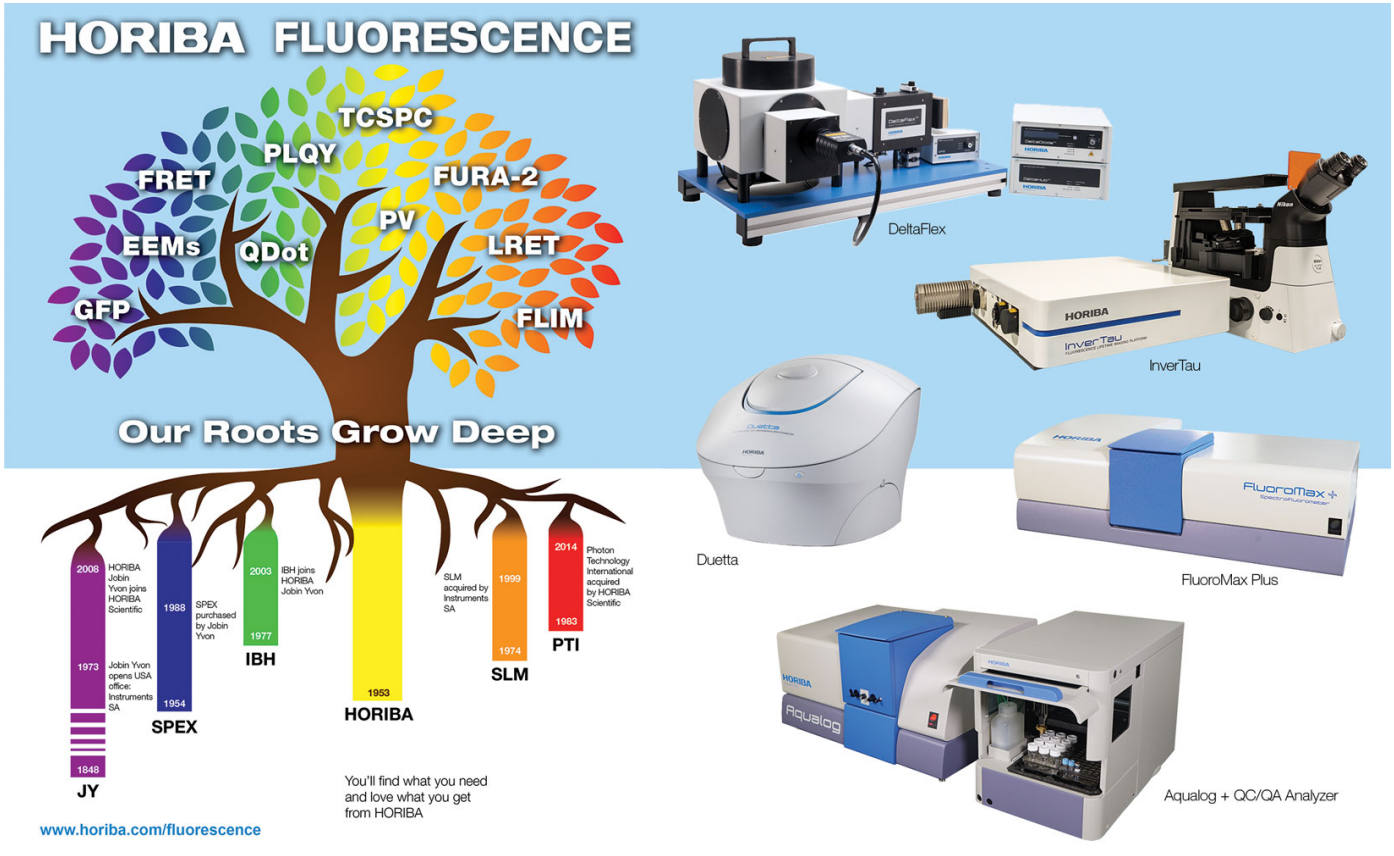
Ion detection in a DNA nanopore FET device

To cite this article: William Livernois *et al* 2024 *Nanotechnology* **35** 325202

View the article online for updates and enhancements.

You may also like

- Towards atom manufacturing with framework nucleic acids
Xiaoliang Chen, Bingjie Yan and Guangbao Yao
- The potential of DNA origami to build multifunctional materials
Kosti Tapio and Ilko Bald
- Effect of anchor positioning on binding and diffusion of elongated 3D DNA nanostructures on lipid membranes
Alena Khmelinskaia, Henri G Franquelim, Eugene P Petrov et al.



This content was downloaded from IP address 74.64.106.200 on 26/08/2024 at 17:10

IOP Publishing Nanotechnology
Nanotechnology 35 (2024) 325202 (11pp) https://doi.org/10.1088/1361-6528/ad460b

Ion detection in a DNA nanopore FET device

William Livernois[1], Purunc (Simon) Cao[1], Soumyadeep Saha[2], Quanchen Ding[1,3], Ashwin Gopinath[4] and M P Anantram[1]

[1] Department of Electrical and Computer Engineering, University of Washington, Seattle, WA, United States of America
[2] Department of Electrical and Computer Engineering, University of Waterloo, Waterloo, ON, CA, Canada
[3] Department of Electrical and Computer Engineering, Carnegie Mellon University, Pittsburgh, PA, United States of America
[4] Department of Mechanical Engineering, Massachusetts Institute of Technology, Cambridge, MA, United States of America

E-mail: willll@uw.edu

Received 14 February 2024, revised 22 April 2024
Accepted for publication 1 May 2024
Published 20 May 2024

Abstract

An ion detection device that combines a DNA-origami nanopore and a field-effect transistor (FET) was designed and modeled to determine sensitivity of the nanodevice to the local cellular environment. Such devices could be integrated into a live cell, creating an abiotic-biotic interface integrated with semiconductor electronics. A continuum model is used to describe the behavior of ions in an electrolyte solution. The drift-diffusion equations are employed to model the ion distribution, taking into account the electric fields and concentration gradients. This was matched to the results from electric double layer theory to verify applicability of the model to a bio-sensing environment. The FET device combined with the nanopore is shown to have high sensitivity to ion concentration and nanopore geometry, with the electrical double layer behavior governing the device characteristics. A logarithmic relationship was found between ion concentration and a single FET current, generating up to 200 nA of current difference with a small applied bias.

Supplementary material for this article is available online

Keywords: DNA origami, nanopore, FET, TCAD, electrical double layer

1. Introduction

Significant strides have been made to integrate biotechnology with semiconductor nanotechnology but the ability to directly interface living cells is still an emerging area of research. Such devices are being developed for interfacing directly with neurons, which can help monitor and treat chronic pain and Parkinson's disease, using materials ranging from silicon-based microelectrodes to carbon nanotubes [1]. While the length scales of typical CMOS devices rival that of most biological systems, transmission of cellular biochemical signals to a biosensor presents significant challenges including biocompatibility of materials and sensitivity at single molecular level. To develop *in-vivo* sensors for measurement on the cellular level, patches have been developed that use sharp microelectrodes to measure action potentials at specific locations near the cell membrane [2]. Though these devices have seen significant improvement, with smaller electrode sizes and direct integration into CMOS chips [3], these extracellular measurements tend to be severely attenuated due to the insulating nature of the cell membrane. Signals can decrease from 10 s of millivolts inside the cell down to 10–100 s of microvolts, significantly reducing the signal to noise ratio of these microelectrode sensors [2, 4].

As an alternative setup, we use an 'artificial gap junction' constructed using a nanopore on a CMOS device as a direct interface between the cell and electronic device (see figure 1(A)). Our proposed device could be directly anchored to the cellular membrane and thus could directly measure intracellular activities rather than relying on extracellular electrode measurements. In this study, we use the dimensions of a DNA origami nanopore constructed in a six-helix bundle topology [5]. Inspiration for using a DNA nanopore comes from naturally occurring transmembrane nanopores, such as the protein Gramicidin, which has been modeled as an ion channel [6]. Such protein nanopores found in nature can

© 2024 IOP Publishing Ltd

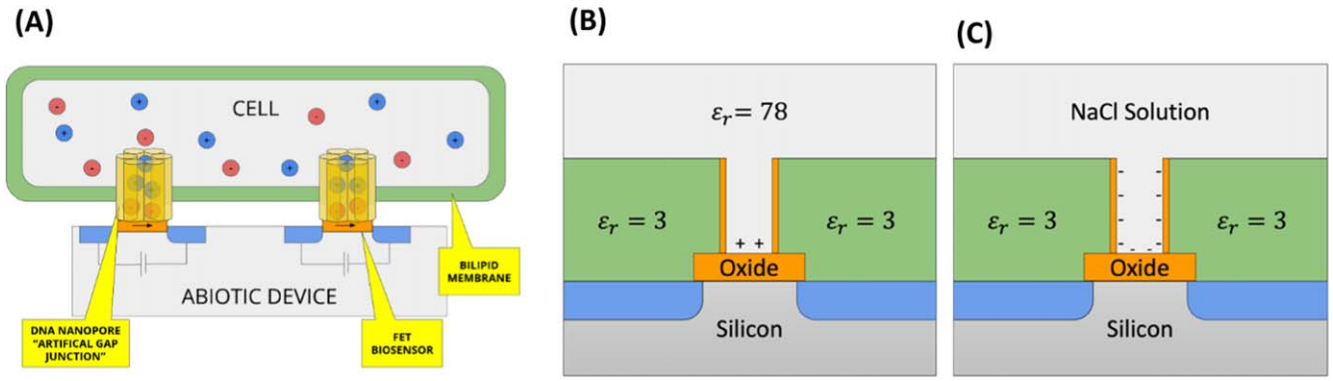


Figure 1. (A) A diagram of a cell connected to the device showing the DNA-origami nanopore channel that acts as the artificial gap junction. Two versions of this device are shown: (B) modeling the electrolyte as an insulator with ions only at the interface and (C) modeling the electrolyte as a semiconductor.

target molecules and block ion current across a membrane, which can be measured experimentally. Not only can the DNA nanopore form a stable trans-membrane pore, like the protein nanopore Gramicidin, but also the self-assembly properties allow it to be customized, varying pore size or integrating the nanopore into a larger device. The DNA-origami structure is bio-compatible and can be modified with ligands to anchor to the lipid bi-layer on a cell, causing minimal disturbance to the cell membrane [7, 8]. This self-assembling structure would be compatible with the living system and convert signals generated by ionic currents directly into an electrical signal using a gated ion-selective FET. This novel device opens a pathway for integration into existing CMOS devices while overcoming issues of non-specific extracellular measurement. While typical nanopore sensors detect single molecules and ions by measuring the change in ion flow across a membrane [9], the proposed device would detect the ions as a buildup of charge across the gate of the FET. A blanket of ions (electrical double layer (EDL)) would form on the nanopore inner wall and over the gate oxide in a manner dependent on the local environment, and the resulting source-drain current can be used to measure the presence of ions in the cell. Using a FinFET geometry and taking advantage of the surface charge of the DNA, we found that the resulting drain current is sensitive to the ion concentration in the nanopore.

To model this setup, we solved the drift-diffusion equations for arbitrary device geometries. This tool allowed us to model the distribution of ions in the gate of the MOSFET and gain a basic understanding of the proposed semiconductor device's biosensing ability. A simplified model was used first, modeling the water in and above the nanopore as an insulator with a dielectric constant of 78. This setup is depicted in figure 1(B), with the ion charge added directly to the interface between the water and the FET. In the second model, depicted in figure 1(C), the ion concentration in the electrolyte was modeled as a semiconductor with the same intrinsic charge carrier concentration and the surface charge of the DNA and silicon oxide surface were modeled based on the solvent interaction. This meant that the gate potential of the FET is controlled by distribution of ions on the negatively charged nanopore and oxide surface. In both studies, the relative dielectric constant of the bilipid membrane (in green, surrounding the nanopore) is taken to be 3 based on experimental results [10]. Using this approach allowed us to first look at the feasibility of integration with existing CMOS technology and check underlying assumptions before assessing the electrical characteristics of the full artificial gap junction device.

2. Methods

2.1. 3D model of FET

As an initial study to determine the overall behavior of this novel device, two standard FET geometries were modeled to determine the sensitivity to the presence of ions. For this study, the ions were modeled as a layer of localized charge under a cylindrical dielectric, on top of the gate oxide, as shown in figure 1(B). In this explorative study involving figure 1(B) we did not consider the surface charge of the DNA nanopore and instead focused on the geometry of the nanopore and FET device and the effects on overall electrical field on the gate. For this reason, counter ions were not included in these simulations with the assumption that they are not nearby and therefore do not have a significant effect on the gating. The *I–V* characteristic of the device was obtained across a range of ion concentrations in the nanopore to demonstrate the sensitivity of each geometry. The device studied next in figure 1(C) however included the effect of counterions.

The first geometry modeled was the planar *n*-channel metal–oxide–semiconductor field-effect transistor (MOSFET). For this MOSFET, the gate is on top of the planar oxide layer on top of the device. The dimensions and doping concentrations were determined relative to values scaled from previously modeled systems [11]. The source and drain were modeled with a gaussian doping profile with the doping concentration dropping to $10^{19}\,\mathrm{cm}^{-3}$ at the channel junction region, see the SI (section 2) for a detailed description. To model the effect of ion density in the nanopore, the gate

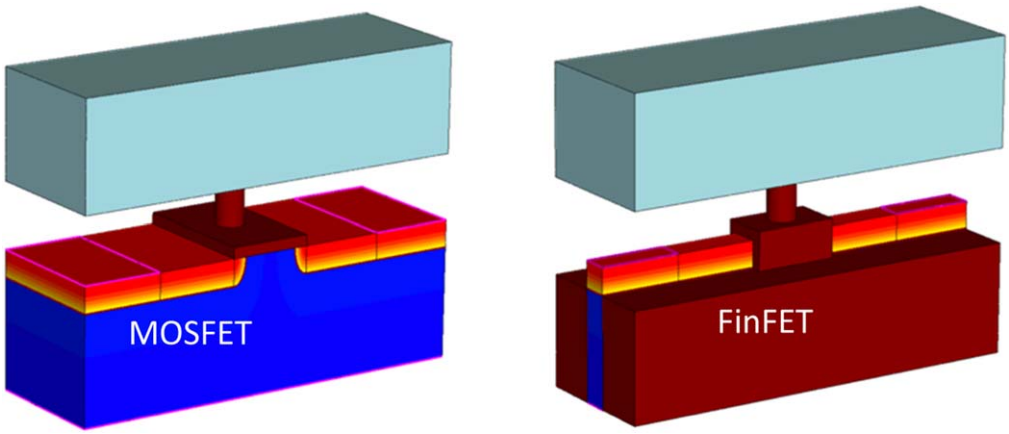


Figure 2. The 3D geometry used for the MOSFET (left) and FINFET (right) geometries. The heatmap shows the doping concentration across the devices. A fully labeled diagram with all dimensions can be found in the SI. The membrane has been removed in the figure to make the nanopore connecting the gate oxide and the light blue solvent box visible.

electrode was replaced with the nanopore structure (see figure 2).

The second geometry modeled was a fin field-effect transistor (FinFET) which demonstrates enhanced gate sensitivity [12]. The FinFET geometry, as depicted in figure 2, causes the electric field in the gate to be more focused around the channel, increasing sensitivity of drain current with gate potential. The geometry and silicon doping were set to match that of the MOSFET, with values given in the SI (table S1). The 3D (three-dimensional) gate geometry is constructed by attaching a substrate of height 20 nm below the channel and the source/drain region. The gate has a total length of 75 nm (nominal channel length of 15 nm and nominal source/drain length of 30 nm with gaussian doping as described in section 3 of the SI) and a cross-section of 5 nm × 5 nm, between two SiO2 slabs. With the FinFET geometry as well, the gate was replaced with the nanopore cylindrical structure.

Both structures were explored by varying the total charge in the nanopore from 1 to 4 ions, which corresponds to a concentration range of 13–52 mM over the whole nanopore volume. To compare the sensitivity between the two topologies the conduction band energy barrier size was compared. Note that device sensitivity requires comparing the relative change in barrier height from the zero-ion case, which directly relates to the change in drain-source current that could be measured experimentally.

2.2. Electrical double layer theory

The transport phenomenon at nanoscale significantly depends on the EDL phenomenon, which forms at the solid–liquid interface due to the electrostatic interaction between ions in solution and surface charges on the solid. These ions arrange themselves into a unique double layer of mobile and immobile ions, which govern the electric field behavior inside a nanopore. Near the surface, the ions opposite to the surface charge polarity (counterions) are attracted, while ions of the same charge (coions) are repelled away. This results in an unbalanced distribution of charged particles and thus the development of an electric potential on the periphery of the surface. The distribution of charges and the potential can be described using the Gouy–Chapman–Stern model (GCS) [13]. According to this model, ions form a bilayer structure: Stern layer and diffuse layer. In the Stern layer, the ions are immobile due to the strong electric field from the surface charges. The plane between the mobile and immobile layer of ions is known as the shear plane and the potential on this plane is known as zeta (ζ) potential, which is an important boundary condition while modeling the EDL.

A nanopore can be modeled using the continuum equations when the length scales are above those of the free ion [10]. The condition for this is determined by a dimensionless constant, called the Knudsen number, defined as the ratio of the ion mean free path to the representative physical length scale of the system. To keep the continuum assumption valid, the Knudsen number for the system should be less than 0.1, where a Knudsen number of 0.1 corresponds to the start of the transition between continuum and discrete models. Considering the mean free path for pure water to be about 0.126 nm (assuming a molecular radius of 2.75 Å) the limit of the nanopore diameter to use the continuum approximation is around 1.3 nm. The nanopore has a diameter of 4 nm, allowing us to apply this approximation in our model. In the continuum regime, the motion of the charged species is determined by diffusion due to Brownian motion and the drift caused by an applied electric field. Another factor which also contributes towards the transport of charged particles is the convection due to fluid flow. For the sake of simplicity, we will assume a steady state condition where the bulk flow velocity of water is zero, making the system completely static and not adding in the effects of ion flow.

Considering a strong electrolyte (e.g. KCl), the transport of the ith ionic species in the system is governed by the Nernst–Planck equation,

$$\frac{dc_i}{dt} + \nabla \cdot J_i = 0 \tag{1}$$

$$J_i = -D_i \nabla c_i - \mu_i c_i \nabla \psi \tag{2}$$

where c_i is the concentration of the ith ionic species, J_i is its flux density, D_i the diffusivity, μ_i the mobility and ψ is the electrostatic potential. The diffusivity and mobility of the

electrolyte can be related using the Einstein relation given by

$$\frac{D_i}{\mu_i} = \frac{kT}{z_i q} \tag{3}$$

where, k is the Boltzmann constant, T is the absolute temperature, q is the elementary charge and z_i is the valence of that ionic species. These equations are similar to the drift-diffusion equations used to model semiconductors. To model the EDL potential and ionic distribution for an infinitely long nanopore, equations (1) and (2) need to be simplified further under equilibrium. If we consider the cylindrical coordinate system (r, ϕ, z) symmetric to a cylindrical nanopore, the EDL will form along the wall of the nanopore, radially inward, while the transport will occur along the z-direction. Assuming that the current flow is zero in the radial direction, equations (1) and (2) will simplify to,

$$\frac{1}{r}\frac{d}{dr}\left(-rD_i\frac{dc_i}{dr} - r\frac{z_i q D_i c_i}{kT}\frac{d\psi}{dr}\right) = 0 \tag{4}$$

Integrating equation (4) and assuming that $\left(\frac{d\psi}{dr}\right)_{r=0} = 0$ and $\left(\frac{dc_i}{dr}\right)_{r=0} = 0$, we get,

$$\frac{z_i q}{kT}\frac{d\psi}{dr} + \frac{d(\ln c_i)}{dr} = 0 \tag{5}$$

which relates the electric potential with the ionic concentration. In the case of a thin EDL compared to the radius of the nanopore, the bulk characteristics of the electrolyte can be assumed near the center of the nanopore. Applying the boundary conditions $(\psi)_{r=0} = 0$, $(c_i)_{r=0} = c_{i0}$ and integrating equation (5), we get the Boltzmann distribution of ions,

$$c_i = c_{i0}\exp\left(-\frac{z_i q\psi}{kT}\right) \tag{6}$$

where c_{i0} is the bulk concentration of the ith ionic species. Solving the Boltzmann distribution coupled with the Poisson's equation,

$$\nabla(\varepsilon_r\varepsilon_0\nabla\ \psi) = -q\sum z_i c_i \tag{7}$$

gives the potential and ionic distribution in a nanopore, where ε_r is the relative permittivity of the solvent and ε_0 is the permittivity value of free space. This Poisson Boltzman (PB) model is commonly used as a simplified model for interface modeling. When applied to the case of the cylindrical nanopore, the boundary conditions are set to $(\psi)_{r=R} = \zeta$ and $\left(\frac{d\psi}{dr}\right)_{r=0} = 0$. This value of the zeta potential (ζ) can be calculated as a function of surface charge (σ) using the Grahame equation [14] which is obtained by integrating equation (6) to get

$$\zeta = \frac{2k_B\ T}{zq}\sinh^{-1}\left(\frac{\sigma}{\sqrt{8c_0\varepsilon_r\varepsilon_0 k_B T}}\right), \tag{8}$$

where c_0 is the bulk concentration of the electrolyte and z is the charge of each ion. The thickness of an EDL is commonly characterized by the Debye screening length (λ_D), the length required for the electric potential of the EDL to drop to $\frac{1}{e}$ times the surface potential (ζ). The expression of this characteristic length can be calculated using

$$\lambda_D = \sqrt{\frac{\varepsilon_r\varepsilon_0 kT}{2q^2 c_0}}. \tag{9}$$

The value of λ_D can be compared directly to the radius of the nanopore to give some indication of the shape of the EDL. When λ_D is much smaller than the nanopore radius, a thin EDL forms with a simple exponential decay. However, if λ_D exceeds the radius of the nanopore, this forms an overlapping EDL, where the interaction of the electric field from the opposite wall of the nanopore must be considered. Since λ_D is a strong function of inverse of ionic concentration, overlapping EDL is common in dilute solutions under nanoconfinement. The overlapping phenomenon results in depletion of coions several orders of magnitude less than the counterions, thereby breaking the overall electroneutrality of the fluid inside the nanopore. This means that bulk characteristics cannot be assumed anywhere inside the nanopore, and a complex model must be considered. We consider this scenario in our 3D modeling, where electroneutrality only occurs outside of the nanopore and the potential caused by the overlapping EDL acts as a gate to the FET. For this scenario, numerical modeling is required.

2.3. Numerical modeling of electrolyte

The Nernst–Planck equation (equation (1)) is an application of the more generic convection–diffusion equation to model ion transport in an electrolyte and is analogous to the drift-diffusion equations used to describe electron–hole transport in a semiconductor. Using the semiconductor transport formulation for a system with a binary electrolyte such as NaCl, positive and negative ion concentrations in an electrolyte are replaced by intrinsic carrier concentrations in a semiconductor. In such a system the bulk electrolyte concentration is given by the intrinsic carrier concentration and any imbalance in positive and negative ion concentration can be represented by doping. The electron or hole mobility can be calculated using the Einstein relation (equation (3)) using the diffusion coefficient for the ions in the electrolyte.

In this study a simple binary electrolyte was used to model the steady state ion behavior to study EDL formation as well as the electric potential of the surrounding system and resulting device characteristic. Applying the 3D drift-diffusion solver to this unique geometry allowed us to look at the non-trivial behavior of the overlapping EDL in the three-dimensional device geometry. In the case of the nanopore, the overlapping EDL occurs when λ_D is equal to or greater than the radius of the nanopore, which means that the ionic concentration at the center is not equal to the bulk concentration and the radial concentration profile deviates from the Boltzmann distribution (equation (6)). However, with the 3D geometry two key assumptions were made about the system: (A) the solvent behaves as a constant dielectric, ignoring dielectric polarization effect for polar solvents, and (B) the ions behave as point charges rather than particles of finite size. This model is referred to as the 3D *model* throughout. To look at the impact of each of these assumptions, further numerical modeling of the system was done for two simplified 1D (one-

dimensional) cases: an infinite charged plane and an infinite cylindrical nanopore. All simulations for the 3D model were based on solving the drift-diffusion equations using the Sentaurus TCAD framework to determine device characteristics of systems with non-trivial geometries. This setup has been used for bioelectronic systems [15–17] with further model enhancements to account for multiple ions [18].

Addressing the first assumption involves modeling the dielectric properties of the solvent as a function of local potential. In the previous sections, we described the EDL considering the solvent as a dielectric medium of constant permittivity. This assumption allowed us to use the field derived equation coupled with the Boltzmann distribution to fully describe the system, and the interaction between solvent molecules and the electric field was neglected. The interaction with the polar solvent can be modeled using a relative permittivity via the Booth's field-dependent permittivity model,

$$\varepsilon_r = n^2 + [\varepsilon_r^0 - n^2]\left[\frac{3}{\beta E}\right]\left[\coth(\beta E) - \frac{1}{\beta E}\right]$$
$$E = \left|-\frac{d\psi}{dr}\right|,\ \beta = \frac{5\mu^p}{2kT}(n^2+2), \tag{10}$$

where, n is the refractive index of the solvent, ε_r^0 is the field-independent relative permittivity of the solvent and μ^p is the dipole moment of the solvent [19, 20]. Booth's model effectively captures the contribution of the polarization field of solvent dipole molecules in the description of EDL. Together with equations (6) and (7), Booth's model (equation (10)) gives a much more complete description of EDL under nanoconfinement. From equation (10), it can be observed that the effective permittivity of the solvent decreases as we go towards the nanopore walls, where the electric field magnitude increases. Thus, the characteristic length of the EDL, which directly depends on the permittivity value, also decreases, thereby altering the ion distribution in the nanopore. This equation can be added as a non-linear term coupled with Poisson's equation to numerically solve for the electric field and resulting ion distributions. In addition, Poisson's equation must be further modified to include the spatial dependence of the permittivity. For the case of the 1D slab, this gives us the expression:

$$\frac{d}{dx}\left(\varepsilon_r(x)\,\varepsilon_0\frac{d\psi}{dx}\right) = \varepsilon_0\left(\frac{d\varepsilon_r}{dx}\frac{d\psi}{dx} + \varepsilon_r(x)\frac{d^2\psi}{dx^2}\right)$$
$$= -q\sum z_i c_i. \tag{11}$$

While each differential can be solved numerically, we can reduce computational complexity by solving this derivative directly, using the chain rule to get:

$$\frac{d\varepsilon_r}{dx} = \frac{d\varepsilon_r}{d\left(\frac{d\psi}{dx}\right)}\left(\frac{d\left(\frac{d\psi}{dx}\right)}{dx}\right) = \frac{d\varepsilon_r}{dE}\left(\frac{d^2\psi}{dx^2}\right), \tag{12}$$

assuming the sign of the electric field, E, is aways positive. This derivative can be calculated analytically from equation (10) to get a highly non-linear differential equation that is only dependent on the electric field and ion concentrations, which can be solved numerically by coupling with the Nernst–Planck equation.

Adding finite ion size to the underlying transport equations allowed us to test the impact of the second assumption. In the previous section the mobility constants (see equation (3)) were used to account for diffusion limited transport without considering the ion size limits that lead to the formation of the Stern layer. To study the limits of finite ion size we used the mean-field lattice gas model, which considered the entropy term derived from considering the configuration space of a lattice of ions. Using the approach in [21], the entropy was determined to be a function of ion concentration given by

$$S_i = k_B \log\left(\frac{c_i {a_i}^3}{1 - \sum_j c_j {a_j}^3}\right), \tag{13}$$

where c_i is the concentration of species i and a_i is the diameter of species i. Our binary electrolyte with two ion concentrations (given by n and p for anions and cations respectively) is accounted for. Accounting for this in the entropy term leads to a modification of the Nernst–Planck equation to get a concentration dependence given by

$$\frac{dc_p}{dx} = \frac{qc_p}{k_B T}(z_n c_n {a_n}^3 + z_p(c_p {a_p}^3 - 1))\frac{d\psi}{dx}$$
$$\frac{dc_n}{dx} = \frac{qc_n}{k_B T}(z_p c_p {a_p}^3 + z_n(c_n {a_n}^3 - 1))\frac{d\psi}{dx}, \tag{14}$$

to be coupled with the Poisson equation [21]. Just looking at the form of this equation, one can see that the interaction between the ion species is considered, whereas setting the finite ion size to zero (a_n and a_p) leaves the original 1D Nernst–Planck equation, independent of the other ion species. Combining this equation with the Booth model (equation (10)) gives us a more complete picture of the physics in the system, which we refer to as the 1D *modified PB model*. This first principles model is used to determine the accuracy of the drift-diffusion 3D model for the nanopore device system. Note that in comparison when we use the term 1D *PB model*, it refers to equation (14) in the limit where the finite ion size effect is neglected ($a_n = a_p = 0$) and the dielectric constant is electric field independent.

The 1D model of the EDL were solved both for a single cartesian coordinate, representing EDL formation on a planar substrate, and a single radial coordinate, representing EDL formation in an infinite cylinder (referred to as the *infinite cylinder model*). This allowed for the drift-diffusion and Poisson equations to be combined into 4 different coupled ordinary differential equations solving for the cation concentration, anion concentration, electric potential, and electric field along the given dimension. To solve the boundary value problem the system was set up as an optimization problem to minimize the error of the boundary conditions as a function of the initial condition. In the case of the planar substrate, the bulk concentrations, edge potential ($\psi = 0$), and zeta potential (calculated from equation (8)) were optimized to fit the differential equations. Though the Grahame equation for zeta potential assumes the case of non-overlapping EDL, which is

only true for the 1D semi-infinite slab setup, the resulting values were found to match up well with the 3D model results as an approximation for the overlapping case. The nanopore charge density used to calculate the zeta potential was found from the density of phosphates facing inward in the six-helix bundle. Based on a base pair spacing of 3.4 Å for B-DNA and an average of 6 phosphates facing the inside of the 4 nm diameter pore, the charge density was calculated to be

$$\sigma = \frac{6\cdot(-1)\mathrm{q}}{\pi\cdot 4\mathrm{nm}\cdot 3.4\text{Å}} = -1.4\times 10^{14}\frac{\mathrm{q}}{\mathrm{cm}^2}. \tag{15}$$

Along with this boundary condition, the mid-pore concentrations were used as inputs for the cylindrical nanopore case, matching up the zero electric field mid-pore constraint with the zeta potential at the nanopore surface. The geometries used for 1D and 3D models are in the SI (Figure S3). The boundary conditions for the 1D Model were applied by minimizing the L2 norm of the error after applying a guess initial condition.

2.4. 3D modeling

As a comparison to the developed numerical model for a 1D semi-infinite slab (referred to as the *infinite slab model*) based on Gouy–Chapman theory, a 3D model large enough to remove edge effects was modeled. The slab was made of a 50 × 50 nm semiconductor material with 20 nm length (referred to as *slab model* in the text). An additional oxide was placed on top of the slab with a defined charge density. The electron and hole concentrations corresponding to the bulk semiconductor was modified to represent the ion concentrations of a binary electrolyte (NaCl in this case). The intrinsic carrier concentration was set exactly equal to the concentration of NaCl in the electrolyte, with hole concentration in the simulation representing the concentration of Na^+ ions and electron concentration representing the concentration of Cl^- ions. This intrinsic carrier concentration was adjusted corresponding to the concentrations tested, initially for 200 mM of NaCl. Similarly, the mobilities used for holes (Na^+) and electrons (Cl^-) were based on the reported diffusion constants of Na^+ and Cl^- [22]. The dielectric constant of the semiconductor was set to a constant value of 78 (the same as water). Finally, all dependence of material properties on the band gap, temperature, and local hole/electron concentration were turned off.

As a next step an isolated cylindrical structure with the surface charge and approximate geometry of the six-bundle DNA nanopore was modeled with the electrolyte properties using the 3D model. This was accomplished by placing two reservoirs at each end of the device and solving for the steady state electric potential as well as the ion concentrations. The resulting concentration and electric potential profiles were compared, matching up the 3D model results with the 1D *PB model* and comparing the profiles to the 1D *modified PB model*. The 1D models (slab and infinite nanopore) used to validate the corresponding 3D models (finite slab and finite nanopore connected to two solvent reservoirs on the top and bottom) are shown in figure S3. This figure also shows the boundary conditions used for the 1D model.

In the final device geometry, the cylindrical nanopore 3D model was combined with the previously modeled FinFET geometry, replacing the fixed charge surface with electrolyte. The top electrode gate was replaced with the cylindrical structure modeled as the NaCl solution inside the nanopore. Any variation in the surface charge density and electrolyte concentration of the nanopore was reflected in the EDL characteristics, which changed the channel conduction of the underlying FET device.

While the boundary condition for the DNA nanopore can use the surface charge calculated from equation (15), the surface charge of the FinFET must be modeled separately using the charge of a silicon oxide-water interface. Assuming a neutral pH, we used a site-binding model [23] to get the following equation to solve for surface charge (per unit area):

$$\sigma_s = qN_{\mathrm{sil}}\left[\frac{[\mathrm{H}^+]_s^2 - K_aK_b}{[\mathrm{H}^+]_s^2 - K_b[\mathrm{H}^+]_s + K_aK_b}\right]$$
$$\text{with}[\mathrm{H}^+]_s = [\mathrm{H}]\exp\left(-\frac{q\zeta}{kT}\right), \tag{16}$$

where N_{sil} is the areal density of oxygen atoms on the silicon oxide surface, K_a is the surface dissociation constant for the reaction $\mathrm{Subs}-\mathrm{SiO}^- + \mathrm{H}^+ \overset{K_a}{\longleftrightarrow} \mathrm{Subs}-\mathrm{SiOH}$ and K_b is the surface dissociation constant for the reaction $\mathrm{Subs}-\mathrm{SiOH} + \mathrm{H}^+ \overset{K_b}{\longleftrightarrow} \mathrm{Subs}-\mathrm{SiOH}_2^+$ (Subs refers to the silicon oxide substrate). The values of N_{sil}, K_a, and K_b were taken from [24] to be $5\times 10^{14}\mathrm{cm}^{-2}$, 10^{-6}M, and 10^{2}M respectively. The variable [H] represents the concentration of hydrogen in the bulk electrolyte, which is given by the 10^{-pH}M of the bulk electrolyte, and $[\mathrm{H}^+]_s$ is the hydrogen ion concentration at the silicon oxide surface. This equation was solved self-consistently with the Grahame relation (equation (8)) to get $\sigma_s = -1.01\times 10^{14}\frac{\mathrm{q}}{\mathrm{cm}^2}$ in a solution of 0.2 M NaCl at neutral pH (pH = 7). This computed surface charge density was used as the fixed charge at the gate-electrolyte interface in the 3D simulations.

3. Results

The initial studies with a constant charge density in the nanopore clearly indicate that the FinFET geometry has higher sensitivity, as shown in the conduction band plots in figure 3. This design was tested for 0–4 charges present, with resulting conduction band plotted for each of these cases. While the overall conduction band plot is nearly equivalent for the 4-ion case, the difference in conduction band energy from the case without ions presence is substantially higher. The ratio of these barriers is about 25% higher for the FinFET topology, indicating that the fin geometry had a significant effect on gating induced by the ions. Based on this result it is clear that the FinFET topology is more sensitive to ions and this device topology was used for all following cases.

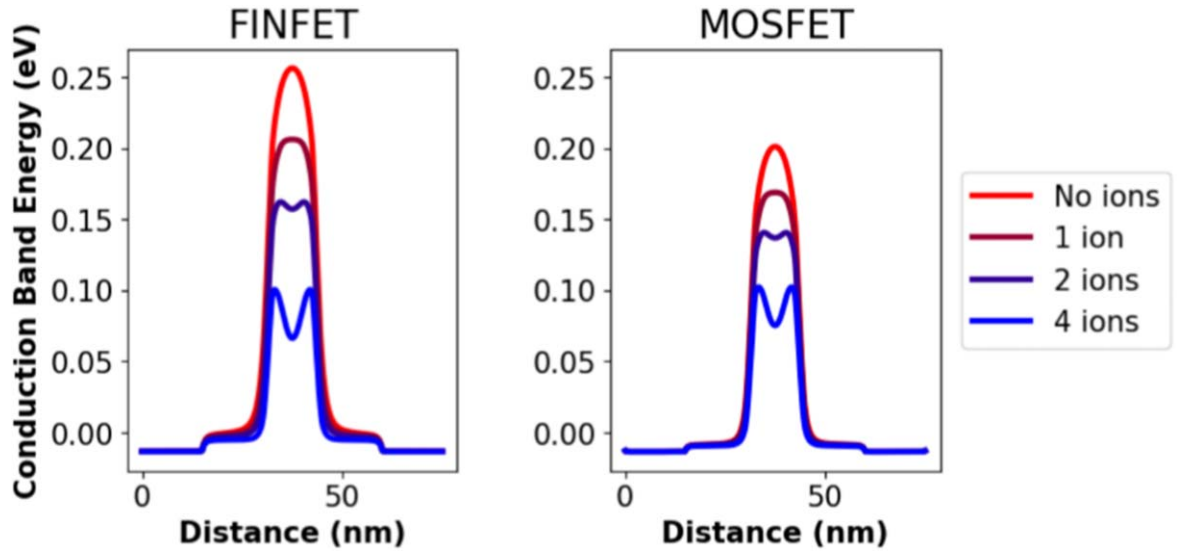


Figure 3. A comparison of the conduction bands of the MOSFET and FinFET geometries varying the ion count in the nanopore from the 3D model. The cutline is along the channel at the center of the device and 0.1 nm below the gate oxide-silicon interface.

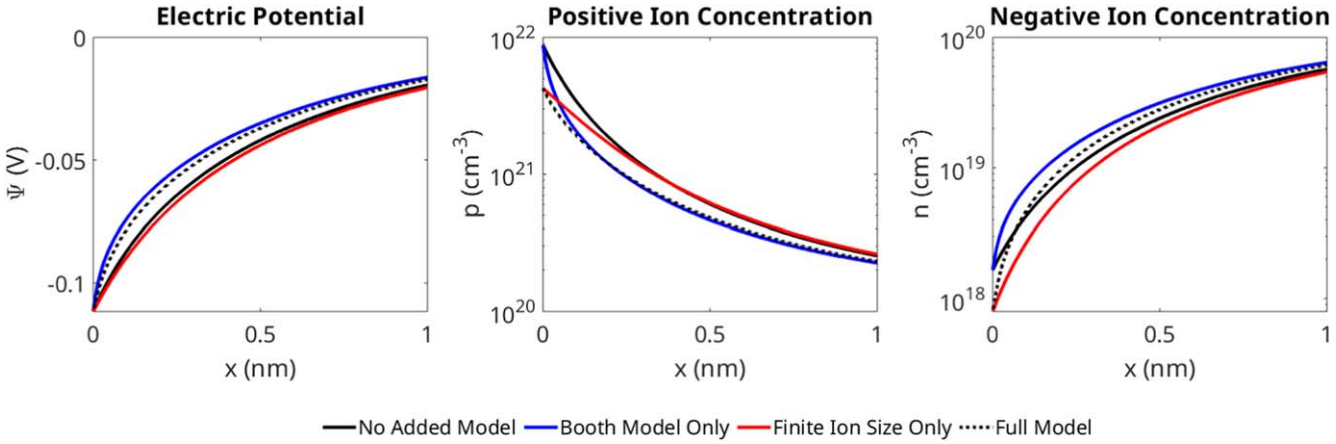


Figure 4. 1D semi-infinite slab model results breaking down the contribution of the finite ion model and the polarizable solvent (Booth) model 1 nm from the surface. The semi-infinite slab was modeled with a 0.2 M concentration of ions and a surface charge equivalent to the DNA nanopore. Note that in these 1D models, No Added Model corresponds to the 1D PB model, and Full Model corresponds to the 1D modified PB model which has both the Booth and finite ion size models included.

After implementing the slab and finite cylinder 3D models, the 1D model was matched for a variety of cases calculating the residuals between each model for validation. Both the 3D and the 1D models reproduced the PB model, with deviations of less than 0.1% between them. Modifying the 1D PB equations to include the finite ion size and Booth models cause the potential and concentration curves to shift, as shown in figure 4. In these graphs, each curve was calculated by selectively turning off the finite-ion and Booth models to plot the potential. This shows that finite ion size limits the concentration as you get closer to the charged surface, contributing a small reduction in the slope of the electric potential (red and solid-black lines on the electric potential plot). However, this effect on the potential was overshadowed by the Booth model, which contributes a larger increase in the slope of the electric potential due to the changing dielectric constant. The residuals (normalizing the difference to the value for the 3D model) are included in section 5 of the SI. The finite ion size had a larger impact on the concentration at the slab-electrolyte interface, where ions accumulate due to the higher electric field, with concentration differences up to an order of magnitude at the interface. The Booth model was found to have a larger effect on the electric potential farther out from the slab, as a direct modification of the dielectric constant's dependence on the electric field.

The results from the cylindrical pore are similar to the slab model case, also incorporating the effects of an overlapping EDL, as shown for the smaller radius cases in figure 5. The surface potential calculated using the Grahame equation, which does not include overlapping EDL effects, was found to mostly match the calculated surface potentials in the nanopore case (see section 4 in the SI for a more detailed explanation). To compare the 1D and 3D cylinder cases, the 1D cylinder model used both (i) the concentration at the center of the nanopore and (ii) the electric potential at the nanopore/electrolyte interface from the 3D model, as

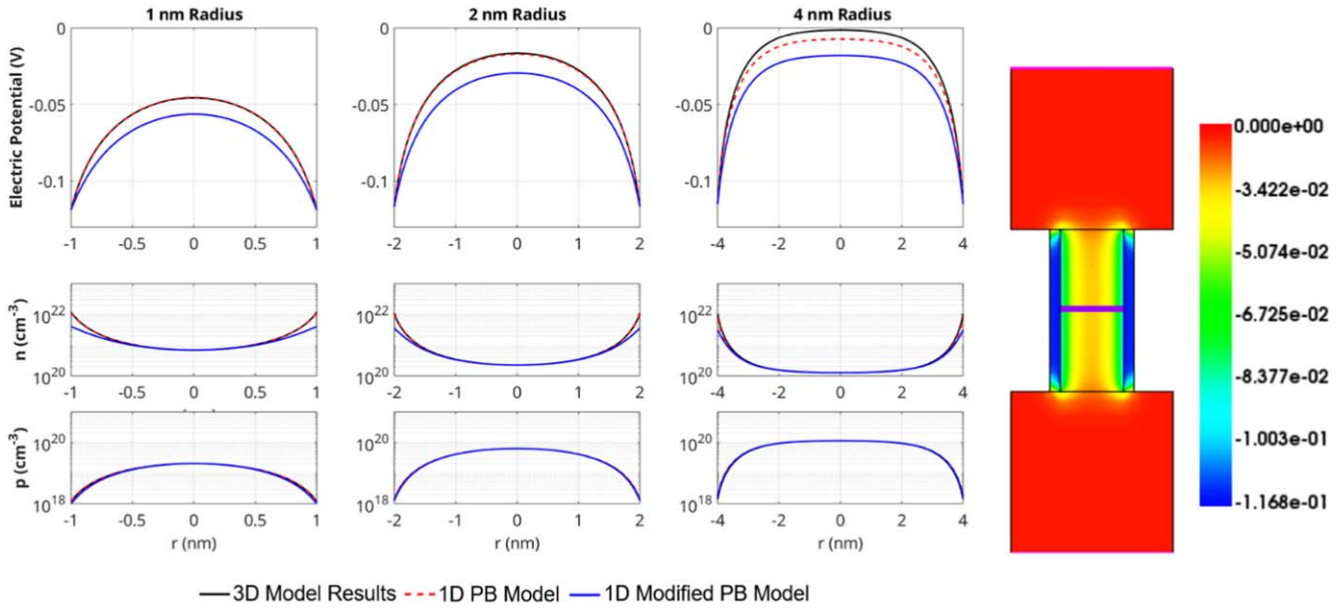


Figure 5. Cylindrical nanopore results comparing the modified PB model (1D simulation of infinite cylinder model) with the 3D drift-diffusion simulation at the cut section of the geometry shown in the right figure. The right figure shows a heatmap of the electrical potential across the nanopore, with the cut section shown in purple. The color bar shows the electrostatic potential in Volts.

Table 1. A comparison of the 3D model results and the 1D PB and modified PB models, showing the percent deviation and EDL voltage drop in the center of the pore.

Pore radius	PB model residual $\left\lvert\frac{\Delta V_{\mathrm{PB,3D}}}{\Delta V_{\mathrm{PB,1D}}}-1\right\rvert$	Modified PB residual $\left\lvert\frac{\Delta V_{\mathrm{MPB,1D}}}{\Delta V_{\mathrm{PB,1D}}}-1\right\rvert$	Voltage drop $\Delta V_{\mathrm{MPB,1D}}$	Knudsen number $K_n=\frac{l_{\text{mean free path}}}{R_{\text{pore}}}$
1 nm	0.3%	14.7%	62.6 mV	0.063
2 nm	0.6%	12.5%	87.0 mV	0.031
4 nm	5.6%	10.0%	96.9 mV	0.016

boundary conditions. Using these constraints, the maximum potential differences between the 1D and 3D models (black and dashed red lines in figure 5) was also found to be less than 1% for all cases except for the 4 nm radius nanopore case shown in the first column of table 1, indicating near equivalence between the finite element solver and 1D differential equation solver. We attribute the deviation between the 1D and 3D models in the 4 nm radius case to the breakdown of the infinite cylinder assumption. The height of the nanopore is only 10 nm (close to the 8 nm diameter) and the axial change in potential is not negligible near the center of this pore. Adding the finite ion and polarizable solvent models led to a consistent drop of 10%–15% in electric potential for all three nanopore sizes (black and blue lines in figure 5). This means that while the 3D model slightly overestimates the potential drop caused by the EDL it was consistent across relevant geometries and ion concentrations to be used for a biosensor.

As a second check of the 3D model, electrolyte-oxide interface was compared as a function of the spacing between the nanopore edge and the oxide, to look at the edge effects on the electric potential. In all other cases the nanopore was positioned to be in contact with the FET surface, with the charged surface of the silicon oxide creating a circular interface at the bottom of the nanopore, whereas this setup included a small gap between the nanopore edge and FET surface filled by the modeled electrolyte solution. To test the effect of the nanopore alignment on the induced gate potential, several spacings were tested with two cases shown in figure 6. The spacing of the nanopore and oxide surface was shown to drastically impact the electric potential on the gate, indicating that minimizing the nanopore-oxide gap is necessary for a sensitive device.

To confirm the effects of pH on the sensitivity of device, the charge of the oxide surface was modulated as determined by the coupled Grahame (equation (8)) and surface charge (equation (16)) equations. The charge of the silicon oxide surface varied substantially across this range, with neutral pH (pH = 7) representing an inflection point between a neutral surface at low pH (all sites are SiOH) and a fully saturated surface at high pH (all surface sites are SiO-). This represents a surface negative charge concentration range from 0 to $5 \times 10^{14} \frac{\mathrm{q}}{\mathrm{cm}^2}$, where the latter concentration is equivalent to the N_{sil} variable given in equation (16). Going to these extreme limits of the surface charge of the oxide layer was found to vary the source drain current by 20% in 0.2 M NaCl. For the smaller pH range typically seen in a cell, this change would be diminished, and choosing a material with different surface chemistry would also alter this effect.

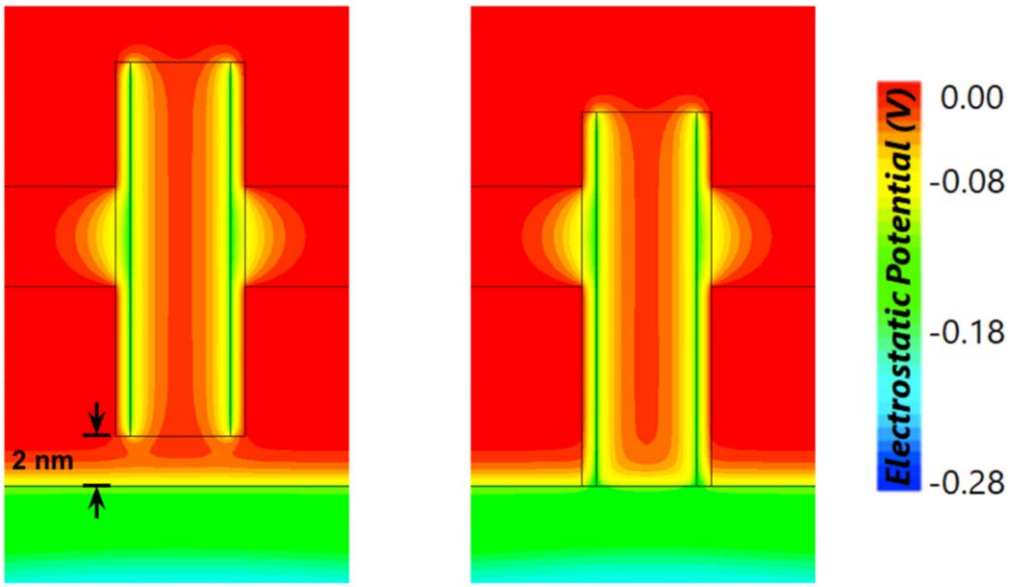


Figure 6. The effect of nanopore spacing on induced gate potential (3D model). The spacing of 2 nm corresponds to the Debye length of the system, showing that a low gap is crucial for ion sensing.

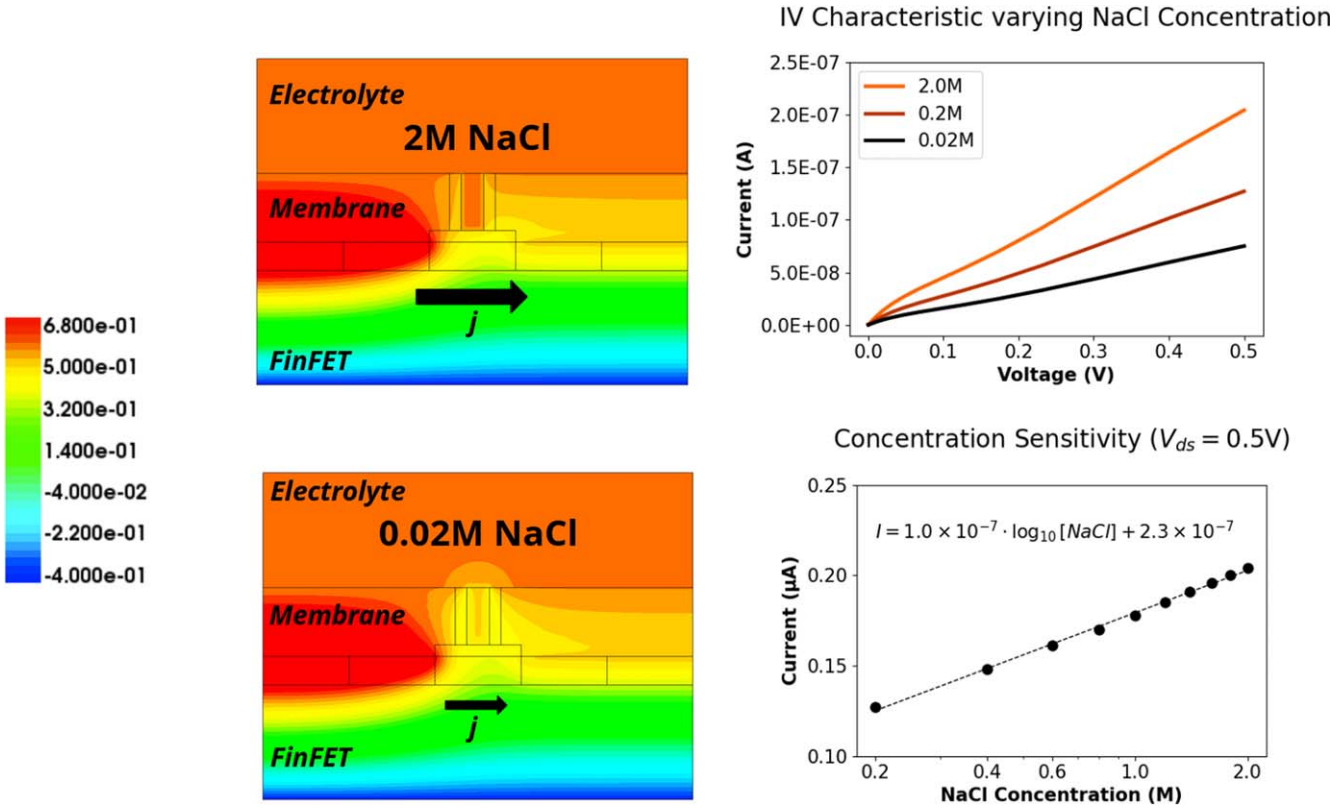


Figure 7. Final 3D model device characteristic showing a high sensitivity to ions that follows a logarithmic relationship with ion concentration. The calibration curve formula is shown as an inset on the bottom right plot, with units of molar for the concentration and amps for the current. The color bar shows the electrostatic potential in Volts.

Applying these models to the combined device we showed that the FinFET geometry increased sensitivity to ion concentration as shown in figure 7. The current through the FET as a function of ion concentration are within a measurable range (between 50 nA and 0.1 μA), indicating that nanopore ion detection is feasible. In addition, we see a logarithmic relationship between ion concentration and drain current, meaning that with a constant applied bias (0.5 V), there is a linear change in current for each order of magnitude change in concentration. A calibration curve has been constructed using a linear regression ($R^2 > 0.999$) and the formula is given as an inset to the sensitivity plot in figure 7.

4. Conclusion

Our results show that single ion detection is possible in the proposed DNA nanopore/FET hybrid nanoscale device, with increased sensitivity using the FinFET topology over a standard MOSFET design. Using the FinFET geometry we showed that the surface charge of the DNA nanopore creates an overlapping EDL that acts as a gate to the FET. This effect was demonstrated both in the 3D drift-diffusion solver and in the 1D model, which matched up directly with direct solutions of the Poisson and Nernst–Planck equations. Using this comparison, we were able to demonstrate that the 3D results are grounded in the EDL theory, showing that the model can be applied to arbitrary geometries such as the proposed artificial gap junction device.

Additional levels of theory were added to improve the accuracy of the model by accounting for finite ion size and polarization of the electrolyte. While this work did not directly compare to experiment, the modified PB model used to analyze the EDL behavior were developed based on experimental results. For instance, the Booth model has been shown to be effective in nanoconfined spaces, accurately reproducing the measured potential from experiment [25]. In addition, the finite ion size model was developed to address unrealistically high concentrations predicted near the interface and has been validated directly with experimental nanoconfined systems [26]. While accounting for these properties of the electrolyte did have noticeable impact on the electrolyte properties, especially in the infinite slab model as shown in figure 4, the overall effect on the electrostatic potential drop in the nanopore was small. Comparing with multiple geometries and ion concentrations the modified model was found to drop the overall EDL potential by around 10%–15% in all cases, proving that the simpler model used by the 3D simulations provides a reasonable estimate of nanopore ion interactions in the nanopores considered. When the 3D model was used to model ion distribution in the full device, the proposed topology shows high sensitivity to ion concentration change and shows promise as a direct probe across a biotic interface.

In this exploratory work, not only do we demonstrate that ion sensitivity is feasible in this proposed device, but we also show that it is more sensitive than existing technologies. The change in current generated by a small ion concentration could be easily measured and is significantly higher than typical noise levels associated with microelectrode arrays used for this application. For comparison, the conduction band energy changes by 10 s of millivolts as shown in figure 3 whereas extracellular microelectrode arrays must be sensitive to a microvolt of potential [4]. Another important result from this study is the sensitivity of a nanopore FET device to the ion concentration. It is clear from our results that any ion concentration fluctuations could contribute significantly to the gate potential on a FET, which is an important consideration for DNA origami-based devices.

Our simulation and results were limited to static (steady state) ion concentrations in a simple binary electrolyte. In a real biological system, there would be many kinds of ions and organic molecules present, which may impact the sensitivity of the device. Previously developed models can be implemented for modeling systems with many types of ions using a simple semiconductor [13] but these may not properly account for larger molecules or chemical reactions that may occur in the system, such as water dissociation. This study was limited to electrical interactions with isotropic dielectric materials, future works can build on this model to look at the interactions between the DNA bundles and the membrane to include any effects that my cause ion buildup or variable dielectric behavior. This work can provide a starting point for future explorations of more complex nanopore sensors, especially in the context of bridging semiconductor devices with biological systems.

Acknowledgments

Research funded by National Science Foundation Grant No. Award Numbers FMSG 2229131 and ECCS SemiSynBio 2027165, and the National Defense Science and Engineering Graduate Fellowship.

Data availability statement

All data that support the findings of this study are included within the article (and any supplementary files).

ORCID iDs

William Livernois https://orcid.org/0000-0001-8637-1213
Soumyadeep Saha https://orcid.org/0000-0003-4462-3595
Ashwin Gopinath https://orcid.org/0000-0002-2874-9457

References

[1] Fattahi P, Yang G, Kim G and Abidian M R 2014 A review of organic and inorganic biomaterials for neural interfaces *Adv. Mater.* **26** 1846–85
[2] Obien M E J, Deligkaris K, Bullmann T, Bakkum D J and Frey U 2015 Revealing neuronal function through microelectrode array recordings *Front. Neurosci.* **8** 423
[3] Abbott J, Ye T, Qin L, Jorgolli M, Gertner R S, Ham D and Park H 2017 CMOS nanoelectrode array for all-electrical intracellular electrophysiological imaging *Nat. Nanotechnol.* **12** 460–6
[4] Spira M E, Shmoel N, Huang S-H M and Erez H 2018 Multisite attenuated intracellular recordings by extracellular multielectrode arrays, a perspective *Front. Neurosci.* **12** 345667
[5] Burns J R, Stulz E and Howorka S 2013 Self-assembled DNA nanopores that span lipid bilayers *Nano Lett.* **13** 2351–6
[6] Roux B and Karplus M 1991 Ion transport in a gramicidin-like channel: dynamics and mobility | *J. Phys. Chem.* **95** 4856–68
[7] Ohmann A, Göpfrich K, Joshi H, Thompson R F, Sobota D, Ranson N A, Aksimentiev A and Keyser U F 2019 Controlling aggregation of cholesterol-modified DNA nanostructures *Nucleic Acids Res.* **47** 11441–51

[8] Luo L, Manda S, Park Y, Demir B, Sanchez J, Anantram M P, Oren E E, Gopinath A and Rolandi M 2023 DNA nanopores as artificial membrane channels for bioprotonics *Nat. Commun.* **14** 5364
[9] Roozbahani G M, Chen X, Zhang Y, Wang L and Guan X 2020 Nanopore detection of metal ions: current status and future directions *Small Methods* **4** 2000266
[10] Gramse G, Dols-Perez A, Edwards M A, Fumagalli L and Gomila G 2013 Nanoscale measurement of the dielectric constant of supported lipid bilayers in aqueous solutions with electrostatic force microscopy *Biophys. J.* **104** 1257–62
[11] Dennard R H, Gaensslen Fritz H, Yu H-N, Leo Rideovt V, Bassous E and Leblanc A R 2007 Design of ion-implanted MOSFET's with very small physical dimensions *IEEE. Solid. State. Circuits. Soc. Newsl.* **12** 38–50
[12] Wu Y-C and Jhan Y-R 2018 *3D FinFET with Lg = 15 nm and Lg = 10 nm Simulation 3D TCAD Simulation for CMOS Nanoeletronic Devices ed Y-C Wu and Y-R Jhan* (Springer) pp 91–183
[13] Pittino F, Palestri P, Scarbolo P, Esseni D and Selmi L 2014 Solid-State electronics models for the use of commercial TCAD in the analysis of silicon-based integrated biosensors *Solid. State. Electron.* **98** 63–9
[14] Grahame D C 1947 The electrical double layer and the theory of electrocapillarity *Chem. Rev.* **41** 441–501
[15] Passeri D, Morozzi A, Kanxheri K and Scorzoni A 2015 Numerical simulation of ISFET structures for biosensing devices with TCAD tools *Biomed. Eng. Online* **14** S3
[16] Chung I-Y, Jang H, Lee J, Moon H, Seo S M and Kim D H 2012 Simulation study on discrete charge effects of SiNW biosensors according to bound target position using a 3D TCAD simulator *Nanotechnology* **23** 065202
[17] Nair P R and Alam M A 2007 Design considerations of silicon nanowire biosensors *IEEE Trans. Electron Devices* **54** 3400–8
[18] Choi B, Lee J, Yoon J, Ahn J-H, Park T J, Kim D M and Kim D H and Choi S-J 2015 TCAD-based simulation method for the electrolyte–insulator–semiconductor field-effect transistor *IEEE Trans. Electron Devices* **62** 1072–5
[19] Booth F 2004 The dielectric constant of water and the saturation effect *J. Chem. Phys.* **19** 391–4
[20] Booth F 2004 Dielectric constant of polar liquids at high field strengths *J. Chem. Phys.* **23** 453–7
[21] Horng T-L, Tsai P-H and Lin T-C 2017 Modification of bikerman model with specific ion sizes *Comput. Math. Biophys.* **5** 142–9
[22] Vitagliano V and Lyons P A 1956 Diffusion coefficients for aqueous solutions of sodium chloride and barium chloride *J. Am. Chem. Soc.* **78** 1549–52
[23] Bergveld P 2003 ISFET *Theory and Practice IEEE Sensor Conf., Toronto* vol 328
[24] Bandiziol A, Palestri P, Pittino F, Esseni D and Selmi L 2015 A TCAD-based methodology to model the site-binding charge at ISFET/electrolyte interfaces *IEEE Trans. Electron Devices* **62** 3379–86
[25] Das S, Chakraborty S and Mitra S K 2012 Redefining electrical double layer thickness in narrow confinements: effect of solvent polarization *Phys. Rev.*E **85** 051508
[26] Pardon G and van der Wijngaart W 2013 Modeling and simulation of electrostatically gated nanochannels *Adv. Colloid Interface Sci.* **199–200** 78–94